GMR
The Original

IN SILICO EVALUATION OF SULFAMOYL PHENYL DERIVATIVES AS POTENTIAL DPP-4 INHIBITORS FOR THE TREATMENT OF TYPE 2 DIABETES MELLITUS: MOLECULAR DOCKING STUDIES, ADMET PROFILING, AND TOXICITY PREDICTION

KUMUD MADAN[1*], SHIWANI JAISWAL[1, 2], ASHISH SRIVASTAVA[3], CHANDAN MONDAL [1,4], SHWETA YADAV[2]

[1*]School of Pharmacy, Sharda University, Greater Noida, Uttar Pradesh -201310, India. Email: kumud.madan@sharda.ac.in,
[2] Buddha Institute of Pharmacy GIDA Gorakhpur, Uttar Pradesh -273209, India Email: jaiswal27apr@gmail.com, Email: shwetay715@gmail.com,
[3] Pranveer Singh Institute of Technology (Pharmacy), Kanpur, Uttar Pradesh -209305, India Email: srivastava457@gmail.com,
[4] School of Medical and Allied Sciences, Department of Pharmacy, Galgotias University, Greater Noida, Uttar Pradesh-203201, India. Email: chandanmondal.cm@gmail.com,

ABSTRACT

Background: Type 2 diabetes mellitus (T2DM) remains a formidable global health burden, compelling the continuous search for safer and more efficacious therapeutic agents. Dipeptidyl peptidase-4 (DPP-4) inhibitors have emerged as a clinically validated drug class owing to their glucose-dependent mechanism of incretin potentiation, conferring a low intrinsic risk of hypoglycaemia. In the present study, aimed to identify novel sulfamoyl phenyl derivatives as potential DPP-4 inhibitors through computational approaches.
Method: A structurally diverse library of 40 sulfamoyl phenyl derivatives was rationally designed and subjected to comprehensive in silico evaluation, encompassing molecular docking against the DPP-4 crystal structure (PDB ID: 2OQV), ADMET profiling via SwissADME, and multi-endpoint toxicity prediction via ProTox-3.0. Three-dimensional ligand geometries were constructed and energy-minimised using ChemDraw 3D, and docking simulations were executed with AutoDock Vina.
Results: The binding affinities across the series spanned −7.0 to −9.7 kcal/mol. The compounds, L_11 and L_33, achieved scores of −9.3 and −9.7 kcal/mol, respectively — equalling or nearly matching the reference inhibitor Sitagliptin (−9.7 kcal/mol). Both leads engaged the canonical catalytic triad residues SER630, GLU205, and GLU206, together with PHE357 and TYR662, through a combination of hydrogen bonding, hydrophobic contacts, and electrostatic interactions. ADMET analysis confirmed that the majority of compounds comply with Lipinski's rule of five, exhibit high predicted gastrointestinal absorption, and display a bioavailability score of 0.55. Toxicity profiling revealed acceptable preliminary safety windows for several derivatives, although targeted structural optimisation will be required to address hepatotoxic and nephrotoxic liabilities in a subset of analogues.
Conclusion: Sulfamoyl phenyl derivatives, particularly L_11 and L_33, demonstrated promising DPP-4 inhibitory potential with favorable binding affinity and pharmacokinetic characteristics. These findings support their further optimization and experimental validation as tractable lead scaffolds for development of next-generation DPP-4 inhibitors in diabetic management.

KEYWORDS: DPP-4 inhibitors; Type 2 diabetes mellitus; Molecular docking; ADMET profiling; Toxicity prediction; Sulfamoyl phenyl derivatives.

1. INTRODUCTION

Type 2 diabetes mellitus (T2DM) is one of the most pervasive non-communicable diseases of our era, now affecting hundreds of millions of individuals worldwide and imposing extraordinary clinical, economic, and societal costs. Pathophysiologically, the disease is defined by a triad of impaired pancreatic β-cell insulin secretion, peripheral insulin resistance, and dysregulated hepatic glucose output, which — if inadequately controlled — culminates in macrovascular and microvascular sequelae including coronary artery disease, stroke, nephropathy, retinopathy, and neuropathy. Despite a pharmacological armamentarium that encompasses metformin, sulfonylureas, thiazolidinediones, SGLT-2 inhibitors, and GLP-1 receptor agonists, the relentless rise in T2DM prevalence underscores the unmet need for mechanistically novel, well-tolerated agents that address the underlying pathophysiology rather than simply correcting hyperglycaemia (1).
Among the therapeutic targets that have attracted sustained medicinal chemistry interest, dipeptidyl peptidase-4

(DPP-4) occupies a particularly compelling position. DPP-4 is a ubiquitously expressed serine protease responsible for the post-secretory inactivation of the incretin hormones glucagon-like peptide-1 (GLP-1) and glucose-dependent insulinotropic polypeptide (GIP) through cleavage of an N-terminal dipeptide bearing a position-2 alanine or proline (2,3). Because GLP-1 and GIP potentiate glucose-stimulated insulin secretion and suppress inappropriate glucagon release in a strictly glucose-dependent manner, pharmacological inhibition of DPP-4 extends their circulatory half-lives without the hypoglycaemic risk that accompanies insulin secretagogues acting through glucose-independent pathways (4). These mechanistic advantages, combined with a favourable tolerability profile in large cardiovascular outcomes trials, have established DPP-4 inhibitors (gliptins) as a widely prescribed second-line antidiabetic class globally (5).

At the molecular level, DPP-4 — also designated CD26 or ADA-binding protein — is a 766-amino acid type II transmembrane glycoprotein that functions as a homodimer (6,7). Each protomer harbours a catalytic domain whose activity is mediated by the canonical Ser630–Asp708–His740 catalytic triad and an eight-bladed β-propeller domain that, together with the catalytic domain, delineates a spacious yet well-defined active-site cavity (8,9). The high-resolution crystal structure deposited under PDB ID 2OQV in Figure 1 has been instrumental in elucidating the structural determinants of DPP-4 inhibitor binding and has served as the template for numerous structure-based drug design campaigns, enabling the rational optimisation of potency and selectivity (10).

Sulfonamide-containing small molecules represent a structurally privileged chemotype in medicinal chemistry. Their biological activities span a broad spectrum, including antibacterial, anticancer, carbonic anhydrase inhibitory, and acetylcholinesterase inhibitory properties (11-13). Sulfamoyl phenyl derivatives are a subset of this class whose capacity to form multiple directional hydrogen bonds — attributable to their $–SO_2NH_2$ donor/acceptor motif — and to engage in electrostatic interactions positions them as potentially effective pharmacophores for the DPP-4 active site. Notwithstanding this structural rationale, the systematic evaluation of sulfamoyl phenyl scaffolds as DPP-4 inhibitors remains relatively underexplored.

The present study was designed to address this gap. A library of 40 structurally diverse sulfamoyl phenyl derivatives incorporating varied sulfonamide and carboxylic acid fragments was constructed and evaluated computationally. Molecular docking against DPP-4 (2OQV) was performed to rank binding affinities and delineate interaction fingerprints; SwissADME-based ADMET profiling was conducted to assess drug-likeness and pharmacokinetic parameters; and ProTox-3.0-mediated toxicity prediction was carried out to characterise preliminary safety profiles. The integrative computational framework adopted here provides a rational basis for prioritising lead compounds for future in vitro and in vivo validation. The structures of all designed ligands are illustrated in Figure 2.

Figure 1. Three-dimensional crystal structure of the DPP-4 enzyme (PDB ID: 2OQV) retrieved from the RCSB Protein Data Bank, showing the active-site catalytic triad (Ser630–Asp708–His740).

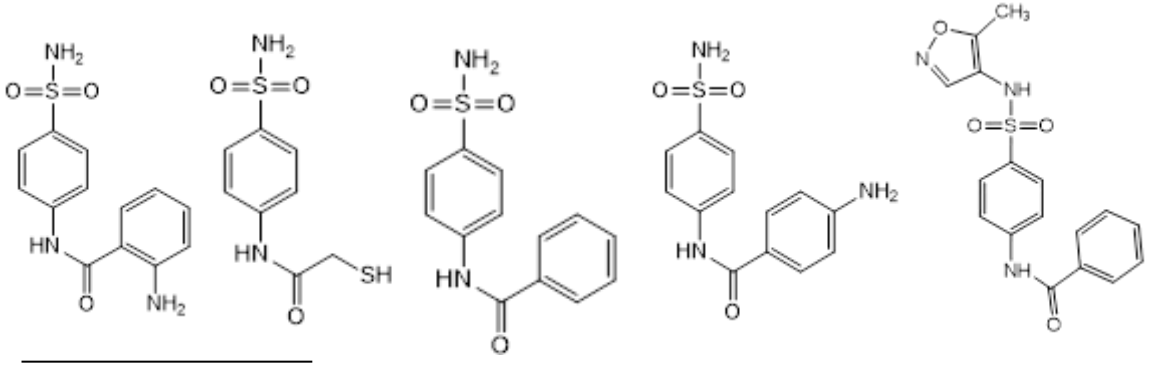

L_2

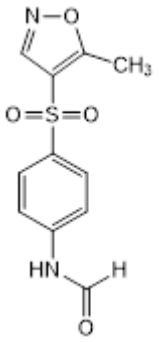

L_3

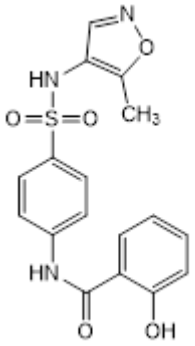

L_5

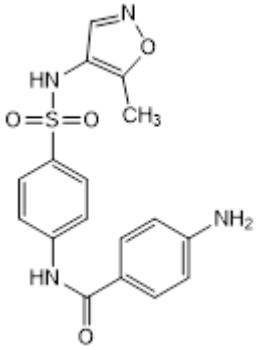

L_8

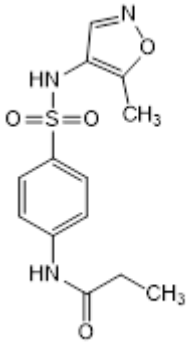

L_11

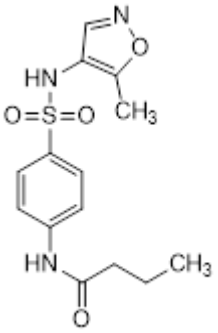

L_12

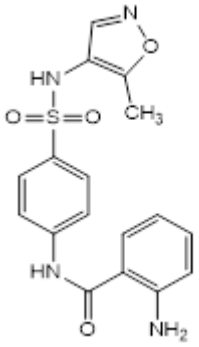

L_14

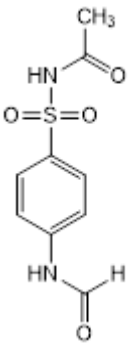

L_15

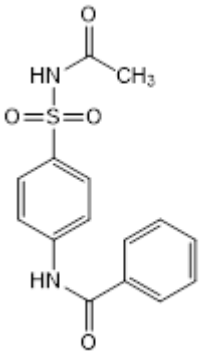

L_16

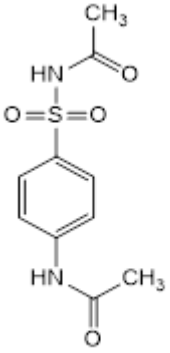

L_17

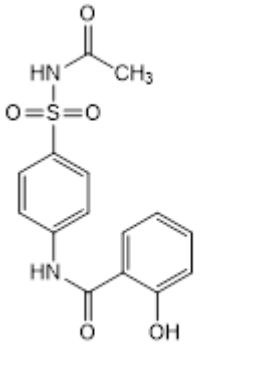

L_19

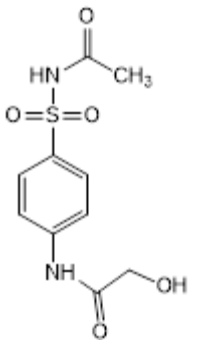

L_21

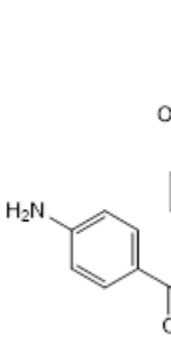

L_22

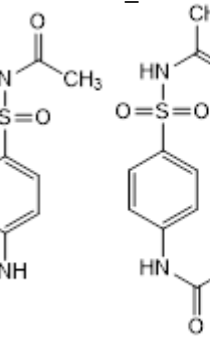

L_23

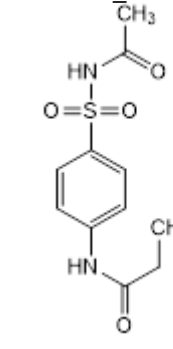

L_24

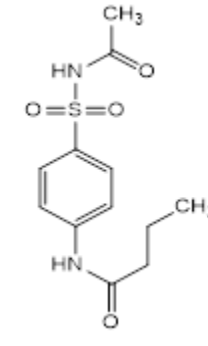

L_25

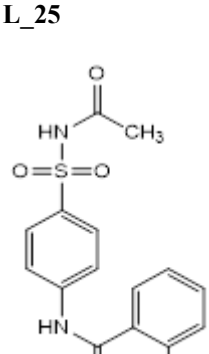

L_26

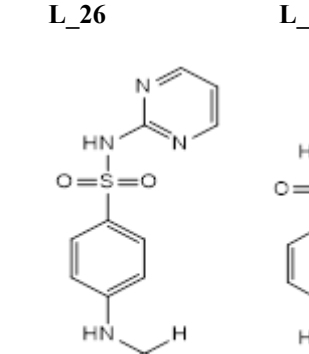

L_27

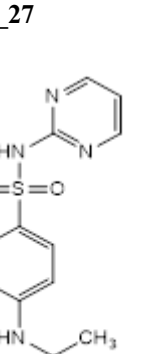

L_28

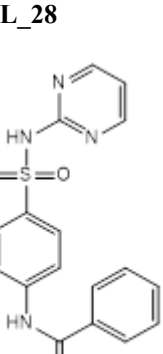

L_29

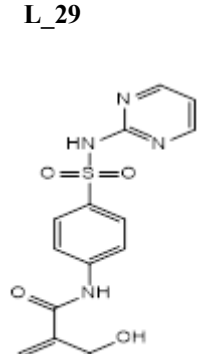

L_30

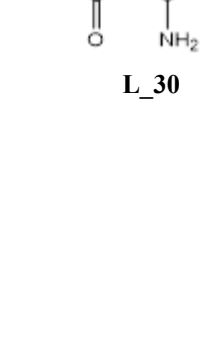

L_31

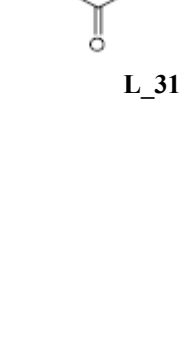

L_32

L_33

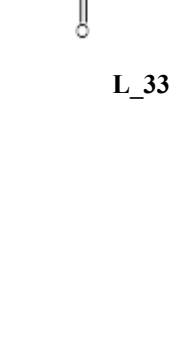

L_34

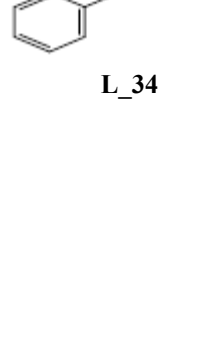

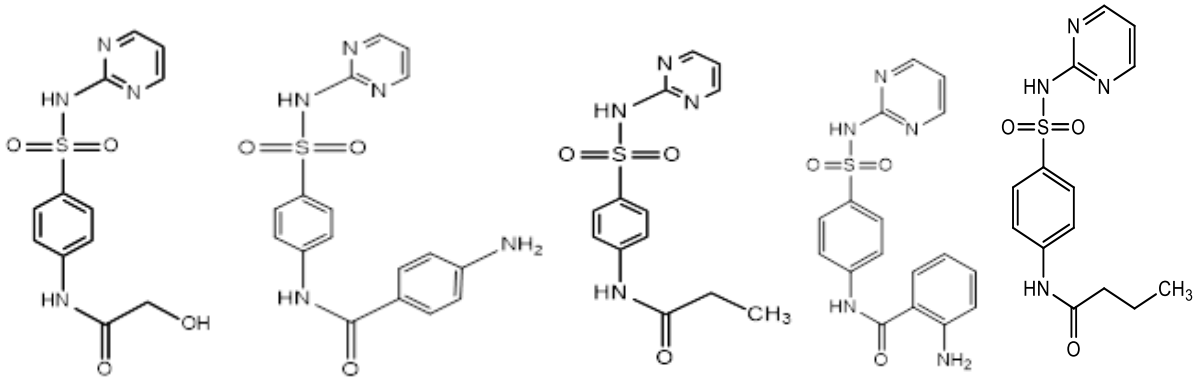

L_35 **L_36** **L_38** **L_39** **L_40**

Figure 2. Chemical structures of the sulfamoyl phenyl derivatives (L_2 – L_40) designed and evaluated in the present study.

2. MATERIALS AND METHODS

Ligand Design and Preparation

A focused library of 40 sulfamoyl phenyl compounds was designed using ChemDraw Ultra 12.0 (14). Structural diversity was introduced by coupling the sulfamoyl phenyl core with a panel of carboxylic acid co-fragments — including para-aminobenzoic acid (PABA), salicylic acid, benzoic acid, propionic acid, glycolic acid, formic acid, acetic acid, thioglycolic acid, and anthranilic acid — via a –CONH amide linkage, yielding the compound series depicted in Figure 2. Each two-dimensional structure was imported into ChemDraw 3D for three-dimensional coordinate generation followed by energy minimisation using the universal force field (UFF). Gasteiger charges were assigned, and rotatable bonds were defined prior to format conversion. The reference DPP-4 inhibitor Sitagliptin was prepared under identical conditions to serve as a benchmark. All compounds were saved in PDB format and subsequently converted to PDBQT format using AutoDock Tools for use in docking simulations.

Protein Preparation

The crystallographic structure of DPP-4 (PDB ID: 2OQV; resolution 2.10 Å) was obtained from the RCSB Protein Data Bank (www.rcsb.org). Protein preparation was performed with AutoDock Tools 1.5.7 (15) in conjunction with BIOVIA Discovery Studio Visualizer. Co-crystallised water molecules and heteroatoms were removed; missing polar hydrogen atoms were added; and Kollman partial charges were assigned. Any incomplete residues were corrected using Swiss-PDB Viewer. The prepared protein was saved in PDBQT format. Grid box parameters were defined by centring the search space on the co-crystallised ligand within the DPP-4 active site, with a grid spacing of 1 Å and centre coordinates of X = 15.296, Y = 54.304, Z = 22.388.

Molecular Docking

Molecular docking simulations were performed using AutoDock Vina. Each of the 40 designed compounds, together with Sitagliptin, was individually docked into the prepared DPP-4 structure under uniform docking parameters. The lowest-energy binding pose for each compound was selected for analysis. Protein–ligand interaction profiles — including hydrogen bonds, hydrophobic contacts, and electrostatic interactions — were visualised and recorded in both 2D and 3D formats respectively in Figure 4 & 5 using BIOVIA Discovery Studio Visualizer. Results are summarised in Table 1.

ADMET and Drug-Likeness Prediction

Pharmacokinetic and drug-likeness properties of all 40 compounds were predicted using the SwissADME web server (www.swissadme.ch). Evaluated parameters included gastrointestinal (GI) absorption, blood–brain barrier (BBB) permeability, cytochrome P450 enzyme inhibition (CYP1A2, CYP2C19, CYP2C9, CYP2D6, and CYP3A4), and skin permeation coefficient (LogKp). Drug-likeness was assessed according to Lipinski's Rule of Five (MW ≤ 500 g/mol, H-bond donors ≤ 5, H-bond acceptors ≤ 10, MlogP ≤ 5). Molecular weight, TPSA, molar refractivity, MlogP, number of rotatable bonds, and counts of hydrogen-bond donors and acceptors were computed and are reported in Table 3. Bioavailability scores were also retrieved from SwissADME. As per Ghose rule, molecular weight range must be 160 to 480 g/mol and molar refractivity 40 to130 (16) and Veber rule predicts the drug molecule should have contain TPSA ≤ 140 and rotatable bond < 10 to exhibit the highest oral bioavailability (17). According to BOILED-Egg Plot (Brain or intestinal estimated permeation method) designed compounds were predicted passive gastrointestinal absorption and BBB penetration. This parameter included two key molecular descriptors like lipophilicity (WLOGP) and TPSA to estimate behaviour of compounds. This plot divide in two region, white region are predicted to high gastrointestinal absorption and yellow region are expected blood-brain barrier penetration of compounds. If compounds falling outside from both regions, that express less likely to exhibit characteristics.

Toxicity Prediction

Multi-endpoint toxicity profiling was conducted using the ProTox-3.0 web server (https://tox.charite.de/protox3). Predicted endpoints encompassed hepatotoxicity, neurotoxicity, nephrotoxicity, respiratory toxicity, cardiotoxicity, carcinogenicity, immunotoxicity, mutagenicity, and cytotoxicity. Predicted LD_{50} values (mg/kg,

oral, rat) were also retrieved. All results are compiled in Table 4.

Table 1. Binding interactions of designed sulfamoyl phenyl derivatives and Sitagliptin with the DPP-4 enzyme (PDB ID: 2OQV)

S. No.	Compound Code	Binding Affinity (kcal/mol)	Interacting Residues	Type of Interaction
1	Sitagliptin	-9.7	SER630, GLU205, GLU206 PHE357, TYR662, VAL656, VAL711, SER630 VAL207, SER630	Hydrogen Bond Hydrophobic Halogen
2	L_2	-7.0	ARG125, TYR547, SER630, ASN710, GLU206, GLU205, SER209 PHE357, TYR666	Hydrogen Bond Hydrophobic
3	L_3	-7.3	HIS126, TYR662, GLU205 TYR662, VAL711 GLU205, GLU206	Hydrogen Bond Hydrophobic Electrostatic (Pi-Anion)
4	L_5	-7.5	ARG125, SER209, ASN710 PHE357 GLU206	Hydrogen Bond Hydrophobic Electrostatic (Pi-Anion)
5	L_8	-7.2	GLN553, ASP545, VAL546, SER552 TYR547 LYS554	Hydrogen Bond Hydrophobic Electrostatic (Pi-Cation)
6	L_11	-9.3	TYR662, GLU205, SER630 PHE357, VAL656, ARG358 GLU206 TYR547	Hydrogen Bond Hydrophobic Electrostatic (Pi-Anion) Other (Pi-Sulfur)
7	L_12	-7.4	GLU205, ARG125, GLU206, TYR662 GLU205, GLU206 (Pi-anion)	Hydrogen Bond Electrostatic
8	L_14	-8.7	SER209, GLU205, ASN710, HIS126 TYR662, VAL711, HIS740 GLU205, ARG125, HIS740	Hydrogen Bond Hydrophobic Electrostatic
9	L_15	-8.1	ARG125, TYR547, SER630, ARG669, ASN710, GLU206, HIS740 TYR662, PHE357, VAL656, VAL711, HIS740 TYR662	Hydrogen Bond Hydrophobic Electrostatic (Pi-cation)
10	L_16	-7.7	SER209, TYR547, TYR662 TYR666 ARG125, GLU205	Hydrogen Bond Hydrophobic Electrostatic
11	L_17	-7.9	ARG356, ARG358, GLU361, SER360 PHE357, ARG356, ILE374, ARG358	Hydrogen Bond Hydrophobic (Pi-Alkyl)
12	L_18	-7.2	ARG125, TYR662, ARG669 ARG125	Hydrogen Bond Electrostatic
13	L_19	-7.5	SER209, TYR547, GLU205 PHE357 ARG125, GLU206	Hydrogen Bond Hydrophobic Electrostatic
14	L_21	-7.1	TYR547, TYR662, ARG669, ASN710, GLU206, GLU205 GLU206	Hydrogen Bond Electrostatic
15	L_22	-8.0	TYR547, TYR662, ASN710, GLU206 PHE357, TYR666 GLU206	Hydrogen Bond Hydrophobic Electrostatic
16	L_23	-7.5	TYR547, TYR662, ASN710, GLU206 TYR666 GLU206	Hydrogen Bond Hydrophobic Electrostatic
17	L_24	-8.5	ARG125, TYR547, TYR662, ASN710, GLU206 PHE357	Hydrogen Bond Hydrophobic
18	L_25	-7.7	TYR662, TYR547, ASN710, GLU206	Hydrogen Bond
19	L_26	-8.7	ARG125, TYR547, GLU205, GLU206 TYR666, PHE357 GLU206	Hydrogen Bond Hydrophobic Electrostatic
20	L_27	-7.1	TYR547, TYR662, ASN710, GLU205 HIS126	Hydrogen Bond Other
21	L_28	-7.5	TYR547, TYR662, ASN710, GLU206 PHE357	Hydrogen Bond Hydrophobic
22	L_29	-7.5	TYR547, TYR662, ASN710, GLU206, SER630	Hydrogen Bond

23	L_30	-8.5	ARG125, TYR547, TYR662, ASN710, GLU206, GLU205 PHE357, TYR666	Hydrogen Bond Hydrophobic
24	L_31	-7.1	ARG125, TYR547, TYR662, ARG669, ASN710, GLU205, GLU206 TYR662, VAL656 GLU206	Hydrogen Bond Hydrophobic Electrostatic
25	L_32	-7.8	ARG125, SER630, TYR662, ARG669, ASN710, GLU206, HIS740 TYR662 ARG125	Hydrogen Bond Hydrophobic Electrostatic
26	L_33	-9.7	ARG125, TYR547, GLU205, GLU206 PHE357, TYR666 GLU206	Hydrogen Bond Hydrophobic Electrostatic
27	L_34	-8.7	ARG125, TYR547, TYR662, ASN710, GLU206 TYR662, PHE357, TYR666, VAL656 GLU206	Hydrogen Bond Hydrophobic Electrostatic
28	L_35	-8.6	ARG125, TYR547, ARG669, ASN710, GLU205, GLU206 TYR662, TYR631, TYR666 HIS740	Hydrogen Bond Hydrophobic Other
29	L_36	-8.5	ARG125, SER630, TYR662, ARG669, ASN710 TYR662, PHE357 ARG125	Hydrogen Bond Hydrophobic Electrostatic
30	L_37	-7.1	ARG125, TYR547, ASN710, GLU206 TYR662, VAL656 GLU206	Hydrogen Bond Hydrophobic Electrostatic
31	L_38	-8.8	ARG125, TYR547, TYR662, ARG669, ASN710 TYR662, VAL656 ARG125	Hydrogen Bond Hydrophobic Electrostatic
32	L_39	-8.6	ARG125, TYR547, TYR662, ASN710, GLU206, GLU205, SER209 TYR662, PHE357, TYR666, VAL656 GLU206	Hydrogen Bond Hydrophobic Electrostatic
33	L_40	-7.6	ARG125, TYR547, ASN710, GLU206 TYR662 GLU206	Hydrogen Bond Hydrophobic Electrostatic

Table 2. Predicted pharmacokinetic properties of designed compounds and Sitagliptin

S. No.	**Ligand**	**GI Absorption**	**BBB Permeant**	**CYP1A2**	**CYP2C19**	**CYP2C9**	**CYP2D6**	**CYP3A4**	**Log Kp (cm/s)**
1	Sitagliptin	High	Yes	No	No	No	No	No	-8.29
2	L_2	High	No	No	No	Yes	No	No	-6.61
3	L_3	High	No	No	No	No	No	No	-7.60
4	L_5	High	No	No	No	No	No	No	-7.15
5	L_8	High	No	No	No	No	No	No	-7.41
6	L_11	High	No	Yes	No	Yes	Yes	Yes	-6.97
7	L_12	High	No	No	No	No	No	No	-7.68
8	L_14	High	No	Yes	No	Yes	No	Yes	-6.93
9	L_15	Low	No	Yes	No	Yes	No	No	-7.54
10	L_16	High	No	No	No	No	No	No	-7.52
11	L_17	High	No	No	No	No	No	No	-7.35
12	L_18	High	No	No	No	No	No	No	-8.33
13	L_19	Low	No	Yes	No	Yes	Yes	No	-7.15
14	L_21	High	No	No	No	No	No	No	-8.55
15	L_22	High	No	No	No	Yes	No	No	-6.91
16	L_23	High	No	No	No	No	No	No	-8.64
17	L_24	High	No	No	No	Yes	No	No	-6.51
18	L_25	High	No	No	No	No	No	No	-9.21
19	L_26	High	No	No	No	No	No	No	-8.42
20	L_27	High	No	No	No	Yes	No	No	-6.91
21	L_28	High	No	No	No	No	No	No	-8.40
22	L_29	High	No	No	No	No	No	No	-8.23

23	L_30	High	No	No	No	Yes	No	No	-7.36
24	L_31	High	No	No	No	No	No	No	-8.15
25	L_32	High	No	No	No	No	No	No	-8.25
26	L_33	High	No	No	No	Yes	Yes	Yes	-7.45
27	L_34	High	No	Yes	No	Yes	Yes	No	-6.46
28	L_35	High	No	No	No	No	No	No	-8.81
29	L_36	High	No	No	No	No	Yes	No	-8.02
30	L_37	Low	No	No	No	No	No	No	-8.21
31	L_38	High	No	No	No	No	No	No	-8.00
32	L_39	High	No	Yes	No	Yes	Yes	Yes	-7.30
33	L_40	High	No	No	No	No	No	No	-7.83

Table 3. Lipinski Rule of Five parameters and LD_{50} values for designed ligands

S. No.	Ligand	MW (g/mol)	TPSA (Å²)	Molar Refractivity	MlogP	Rotatable Bonds	H-bond Donors	H-bond Acceptors	LD50 (mg/kg)
1	Sitagliptin	407.31	77.04	87.25	2.52	6	1	10	2500
2	L_2	291.33	123.66	76.06	0.83	4	3	4	3000
3	L_3	246.31	136.44	59.68	-0.12	4	2	4	5000
4	L_5	276.31	97.64	71.65	1.38	4	2	5	10000
5	L_8	291.33	123.66	76.06	0.83	4	3	4	10000
6	L_11	357.38	109.68	92.80	1.28	6	2	5	3471
7	L_12	281.29	109.68	68.48	0.08	5	2	5	3471
8	L_14	373.38	129.91	94.82	0.76	6	3	6	2300
9	L_15	372.40	135.70	97.20	0.76	6	3	5	3471
10	L_16	309.34	109.68	77.70	0.22	6	2	5	3471
11	L_17	323.37	109.68	82.51	0.49	7	2	5	3471
12	L_18	311.31	129.91	74.06	-0.84	6	3	6	2300
13	L_19	372.40	135.70	97.20	0.76	6	3	5	3471
14	L_21	242.25	100.72	57.24	-0.29	5	2	4	87
15	L_22	318.35	100.72	81.56	1.01	6	2	4	10000
16	L_23	256.28	100.72	61.66	-0.39	5	2	4	87
17	L_24	334.35	120.95	83.58	0.89	6	3	5	2800
18	L_25	272.28	120.95	62.82	-1.19	6	3	5	87
19	L_26	333.36	126.74	85.96	0.48	6	3	4	10000
20	L_27	318.35	100.72	81.56	1.01	6	2	4	87
21	L_28	270.30	100.72	66.46	-0.10	4	2	4	87
22	L_29	284.33	100.72	71.27	0.18	7	2	4	3000
23	L_30	333.36	126.74	85.96	0.48	6	3	4	2800
24	L_31	278.29	109.43	69.04	-0.37	5	2	5	6000
25	L_32	292.31	109.43	73.46	-0.49	5	2	5	1500
26	L_33	354.38	109.43	93.36	0.84	6	2	5	1500
27	L_34	370.38	129.66	95.38	0.32	6	3	6	1500
28	L_35	308.31	129.66	74.62	-1.28	6	3	6	1500
29	L_36	369.40	135.45	97.76	0.32	6	3	5	1500
30	L_37	324.38	148.23	81.39	-0.49	6	2	5	1500
31	L_38	306.34	109.43	78.27	-0.22	6	2	5	1500
32	L_39	369.40	135.45	97.76	0.32	6	3	5	1500
33	L_40	320.37	109.43	83.07	0.04	7	2	5	300

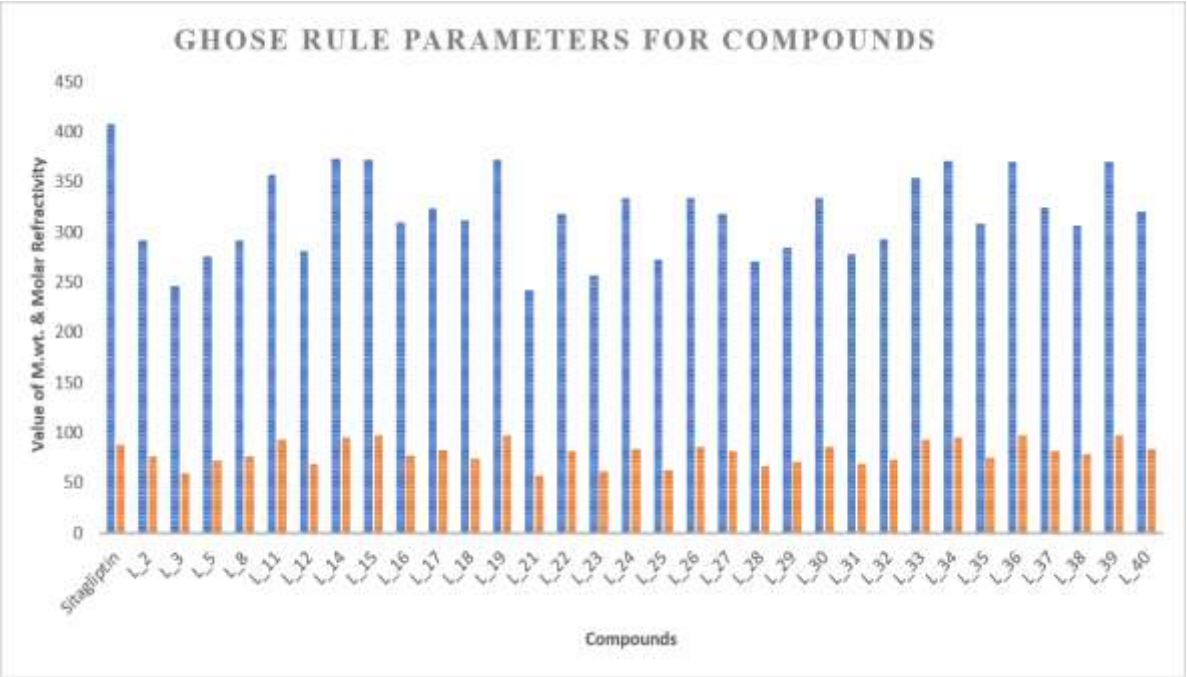

(a) Ghose rule represented blue colour Molecular weight (g/mol) and orange colour Molar refractivity of compounds

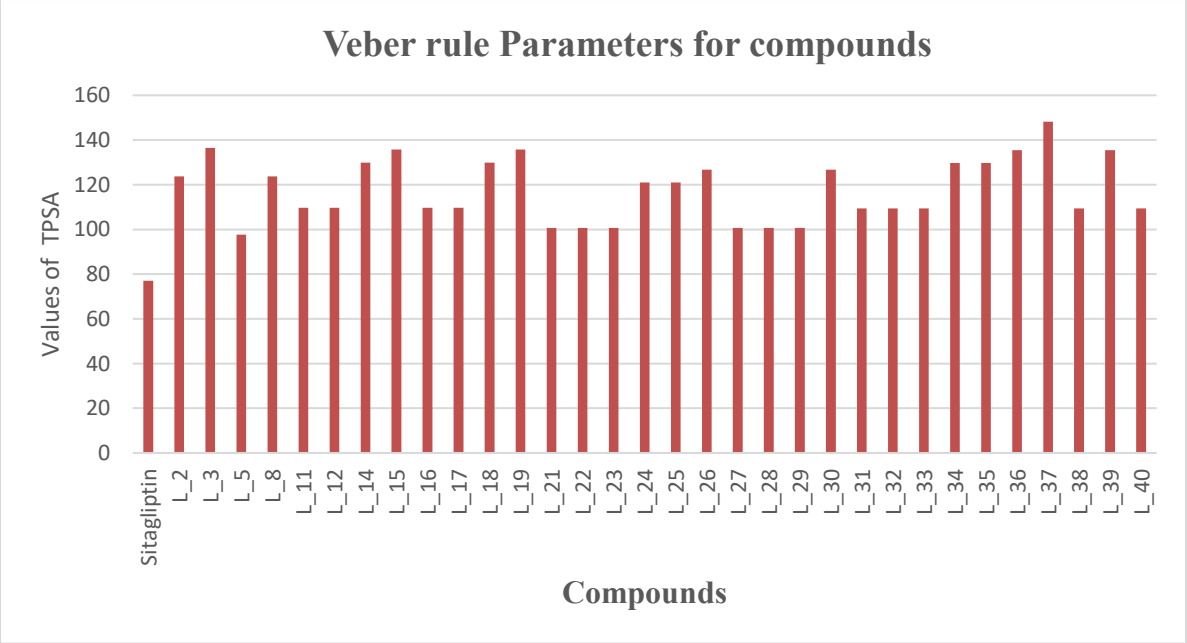

(b) Veber rule represented orange colour TPSA of compounds

Figure 3. Drug-likeness properties represented in graphical format Ghose and Veber rule

Table 4. Multi-endpoint toxicity profiles of designed sulfamoyl phenyl derivatives and Sitagliptin

S. No.	Ligand	Hepato-toxicity	Neuro-toxicity	Nephro-toxicity	Respiratory Toxicity	Cardio-toxicity	Carcino-genicity	Immuno-toxicity	Muta-genicity	Cyto-toxicity
1	Sitagliptin	Inactive	Active	Inactive	Active	Inactive	Inactive	Inactive	Inactive	Inactive
2	L_2	Inactive	Inactive	Inactive	Inactive	Inactive	Active	Inactive	Active	Inactive
3	L_3	Inactive	Inactive	Inactive	Active	Inactive	Inactive	Inactive	Inactive	Inactive
4	L_5	Inactive	Inactive	Inactive	Inactive	Inactive	Inactive	Inactive	Inactive	Inactive
5	L_8	Inactive	Inactive	Inactive	Inactive	Inactive	Inactive	Inactive	Inactive	Inactive
6	L_11	Active	Inactive	Active	Active	Inactive	Inactive	Inactive	Inactive	Inactive
7	L_12	Active	Inactive	Active	Active	Inactive	Inactive	Inactive	Inactive	Inactive
8	L_14	Active	Inactive	Active	Active	Inactive	Inactive	Inactive	Inactive	Inactive
9	L_15	Active	Inactive	Active	Active	Inactive	Inactive	Inactive	Inactive	Inactive
10	L_16	Active	Inactive	Active	Active	Inactive	Inactive	Inactive	Inactive	Inactive
11	L_17	Active	Inactive	Active	Active	Inactive	Inactive	Inactive	Inactive	Inactive
12	L_18	Active	Inactive	Active	Active	Inactive	Inactive	Inactive	Inactive	Inactive

13	L_19	Inactive	Inactive	Active	Active	Inactive	Inactive	Inactive	Inactive	Inactive
14	L_21	Inactive	Inactive	Active	Active	Inactive	Inactive	Inactive	Inactive	Inactive
15	L_22	Inactive	Inactive	Active	Active	Inactive	Inactive	Inactive	Inactive	Inactive
16	L_23	Inactive	Inactive	Active	Active	Inactive	Inactive	Inactive	Inactive	Inactive
17	L_24	Inactive	Inactive	Active	Inactive	Inactive	Inactive	Inactive	Inactive	Inactive
18	L_25	Inactive	Inactive	Active	Active	Inactive	Inactive	Inactive	Inactive	Inactive
19	L_26	Inactive	Inactive	Active	Inactive	Inactive	Inactive	Inactive	Inactive	Inactive
20	L_27	Inactive	Inactive	Active	Active	Inactive	Inactive	Inactive	Inactive	Inactive
21	L_28	Inactive	Inactive	Active	Inactive	Inactive	Inactive	Inactive	Inactive	Inactive
22	L_29	Inactive	Inactive	Active	Inactive	Active	Inactive	Inactive	Inactive	Inactive
23	L_30	Inactive	Inactive	Active	Inactive	Inactive	Inactive	Inactive	Inactive	Inactive
24	L_31	Inactive	Inactive	Inactive	Active	Inactive	Active	Inactive	Inactive	Inactive
25	L_32	Inactive	Inactive	Inactive	Active	Inactive	Active	Inactive	Inactive	Inactive
26	L_33	Inactive	Inactive	Inactive	Active	Inactive	Active	Inactive	Inactive	Inactive
27	L_34	Inactive	Inactive	Active	Active	Inactive	Inactive	Inactive	Inactive	Inactive
28	L_35	Inactive	Inactive	Active	Active	Inactive	Inactive	Inactive	Inactive	Inactive
29	L_36	Inactive	Inactive	Inactive	Active	Inactive	Active	Inactive	Inactive	Inactive
30	L_37	Inactive	Inactive	Inactive	Active	Inactive	Inactive	Inactive	Inactive	Inactive
31	L_38	Inactive	Inactive	Active	Active	Inactive	Inactive	Inactive	Inactive	Inactive
32	L_39	Inactive	Inactive	Active	Active	Inactive	Active	Inactive	Inactive	Inactive
33	L_40	Inactive	Inactive	Active	Inactive	Inactive	Inactive	Inactive	Inactive	Inactive

3. RESULTS AND DISCUSSION

Molecular Docking Analysis

Molecular docking of the 40 sulfamoyl phenyl derivatives against the DPP-4 active site (PDB ID: 2OQV) yielded binding affinities spanning −7.0 to −9.7 kcal/mol (Table 1). Higher (more negative) docking scores reflect thermodynamically more stable ligand–protein complexes and are conventionally interpreted as indicative of greater inhibitory potential in the absence of direct experimental data. The reference inhibitor Sitagliptin docked with a score of −9.7 kcal/mol, engaging SER630, GLU205, and GLU206 through hydrogen bonds and forming hydrophobic contacts with PHE357, TYR662, VAL656, and VAL711 — an interaction fingerprint that is well-precedented in the co-crystal literature and served as the benchmark for assessing the novel compounds.

Two derivatives, L_33 and L_11, emerged as the most promising hits. Compound L_33 achieved a docking score of −9.7 kcal/mol — identical to that of Sitagliptin — whilst L_11 recorded −9.3 kcal/mol, representing a modest but noteworthy difference of only 0.4 kcal/mol from the reference standard. Both compounds recapitulated the key interactions of Sitagliptin: L_33 formed five hydrogen bonds with ARG125, TYR547, GLU205, and GLU206, hydrophobic contacts with PHE357 and TYR666, and an electrostatic (Pi-anion) interaction with GLU206; L_11 established hydrogen bonds with TYR662, GLU205, and SER630, hydrophobic interactions with PHE357, VAL656, and ARG358, and additionally engaged GLU206 through a Pi-anion interaction and TYR547 through a Pi-sulfur contact — the latter an interaction type absent in the Sitagliptin complex that may confer complementary stabilisation within the active site.

A second tier of compounds — L_38 (−8.8 kcal/mol), L_14, L_26, and L_34 (each −8.7 kcal/mol), L_35 (−8.6 kcal/mol), L_39 (−8.6 kcal/mol), L_15 (−8.1 kcal/mol), and L_22 (−8.0 kcal/mol) — exhibited strong binding affinities in the range −8.0 to −8.8 kcal/mol. These derivatives consistently anchored to ARG125, ASN710, TYR547, GLU205, and GLU206, with hydrophobic complementarity provided by PHE357, TYR666, TYR662, and VAL656. The recurrence of these residues across chemically distinct analogues confirms that the sulfamoyl phenyl scaffold exploits the canonical DPP-4 pharmacophore space and does so through multiple interaction modalities.

Interaction frequency analysis revealed that GLU205, GLU206, SER630, ARG125, TYR662, and PHE357 were the most consistently engaged residues across the series. This observation aligns with established structural data on DPP-4 inhibitor binding: GLU205 and GLU206 form the glutamate clamp that coordinates the amino terminus of incretin peptides and is a hallmark interaction for all three structural classes of gliptin; SER630 is the nucleophilic serine of the catalytic triad; and PHE357 and TYR662 define the hydrophobic S1 and S2 sub-pockets that discriminate between DPP-4 and related prolyl peptidases. The ability of the sulfamoyl phenyl scaffold to simultaneously engage hydrogen-bonding, electrostatic, and hydrophobic determinants of the DPP-4 active site is a structurally coherent outcome of the dual hydrogen-bond donor/acceptor character of the $–SO_2NH_2$ group and the aromatic planarity of the phenyl core.

At the lower end of the affinity range (−7.0 to −7.9 kcal/mol), compounds including L_2, L_8, L_3, L_21, L_27, L_31, and L_37 remained compliant with the general interaction pharmacophore but made fewer or weaker contacts — findings that provide structural insight for targeted optimisation of this subset.

ADMET and Drug-Likeness Analysis

Pharmacokinetic and drug-likeness evaluation of the compound library using SwissADME demonstrated that the

vast majority of designed derivatives satisfy Lipinski's Rule of Five criteria: molecular weights ranged from 242.25 to 407.31 g/mol (all ≤ 500 g/mol), MlogP values fell between −1.28 and 2.52 (all ≤ 5), hydrogen-bond donor counts did not exceed 3 (threshold ≤ 5), and hydrogen-bond acceptor counts were ≤ 6 in all cases (threshold ≤ 10) (Table 3). These parameters collectively predict adequate passive membrane permeability and oral bioavailability, which are prerequisite properties for orally administered antidiabetic drugs. As well as Ghose rule, also these compounds are finding drug-likeness properties shown in Figure 3.

Gastrointestinal absorption was predicted to be high for 30 of the 33 evaluated compounds (including the reference). Only L_15, L_19, and L_37 returned low GI absorption predictions — a limitation likely attributable to their relatively elevated TPSA values (135.70, 135.70, and 148.23 Å², respectively), since according to Veber's rule TPSA ≤140 Å² is a well-established threshold associated with impaired intestinal permeation which represented value of TPSA in Figure 3. Notably, none of the designed compounds were predicted to penetrate the blood–brain barrier, a property that may represent a clinical advantage for a peripheral antidiabetic agent by reducing the likelihood of CNS adverse effects and also represented by RADAR in Figure 6.

Cytochrome P450 inhibition profiling revealed that the majority of compounds are unlikely to perturb major CYP isoforms significantly, suggesting a low predicted risk of pharmacokinetic drug–drug interactions — an important consideration given the polypharmacy context in which T2DM medications are typically used. However, a subset of compounds with higher docking scores, including L_11, L_14, L_33, and L_39, showed predicted inhibition of one or more CYP isoforms (CYP1A2, CYP2C9, CYP2D6, and/or CYP3A4). Whilst in silico CYP predictions are directionally informative rather than definitive, these data flag candidates for priority metabolic profiling in experimental follow-up. The bioavailability score for the series was uniformly predicted at 0.55, consistent with moderate oral bioavailability and in line with values reported for marketed oral antidiabetics.

The BOLIED-Egg analysis of designed compounds revealed favorable characteristic properties within the white region, indicating good gastrointestinal absorption which suitability for oral administration as compare to Sitagliptin. So these findings support the drug-likeness of designed compounds shown in Figure 7.

Toxicity Prediction Analysis

Multi-endpoint toxicity profiling using ProTox-3.0 revealed heterogeneous safety landscapes across the series (Table 4). Encouragingly, Sitagliptin itself showed predicted activity for neurotoxicity and respiratory toxicity, providing a calibration reference for interpreting the computational predictions. Compounds L_5 and L_8 returned the most favourable safety profiles, being predicted inactive across all nine toxicological endpoints and returning LD_{50} values of 10,000 mg/kg — consistent with extremely low acute oral toxicity (WHO Hazard Category 5) — which, taken together with their acceptable docking scores (−7.5 and −7.2 kcal/mol), marks them as structurally interesting starting points for optimisation campaigns focused on improving potency whilst preserving their clean toxicity profiles.

A subset of compounds bearing the naphthalene-derived or extended aromatic carboxamide motifs — specifically L_11, L_12, L_14, L_15, L_16, L_17, and L_18 — displayed predicted hepatotoxicity and nephrotoxicity. Whilst computational toxicity models are acknowledged to have significant false-positive rates, the recurrence of these signals across structurally related analogues warrants attention. Hepatotoxicity is among the most common causes of post-marketing drug withdrawal, and flagging at the lead stage permits proactive structural diversification — for example, replacement of electron-rich aromatic systems with saturated or heteroaromatic bio isosteres — before advancing to in vitro cytotoxicity assays. Predicted carcinogenic signals for L_2, L_31, L_32, L_33, L_36, and L_39 similarly underscore the importance of Ames mutagenicity testing and genotoxicity assessment as early experimental triage gates, given the chronicity of antidiabetic therapy.

Respiratory toxicity was flagged for a number of derivatives, whereas cardiotoxicity, mutagenicity, immunotoxicity, and cytotoxicity were largely absent from the majority of compounds — a profile that compares reasonably well with the reference inhibitor. Taken in aggregate, the toxicity analysis identifies a pharmacologically attractive window within the series — particularly around L_5, L_8, and several analogues from the high-affinity cohort — and charts a structure-informed optimisation path for addressing identified liabilities in the remaining compounds.

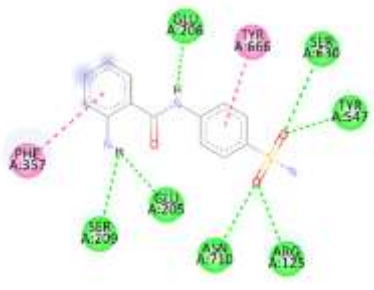

L_2

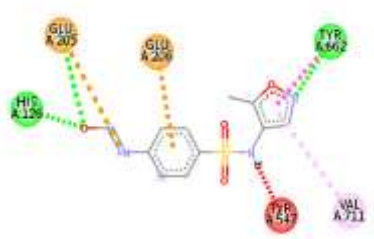

L_3

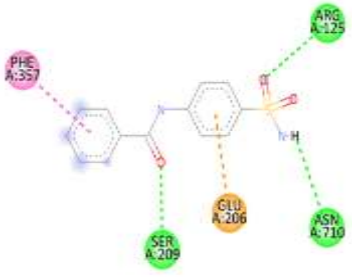

L_5

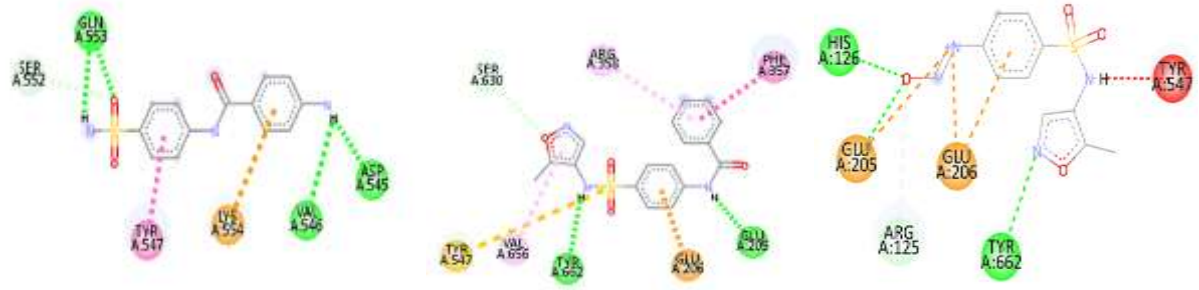

L_8 **L_11** **L_12**

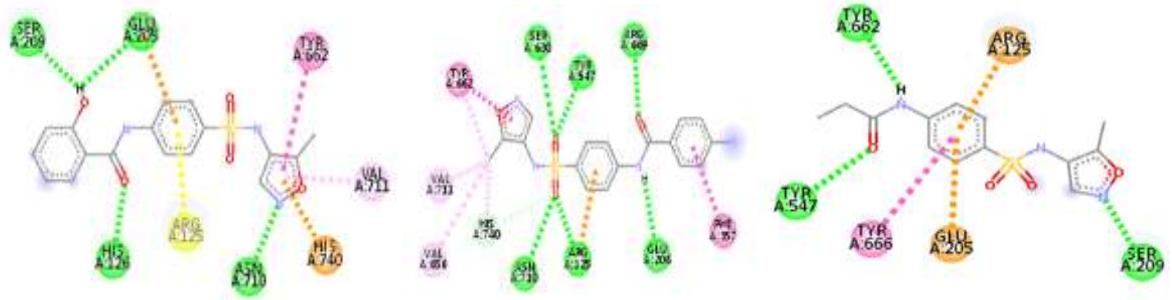

L_14 **L_15** **L_16**

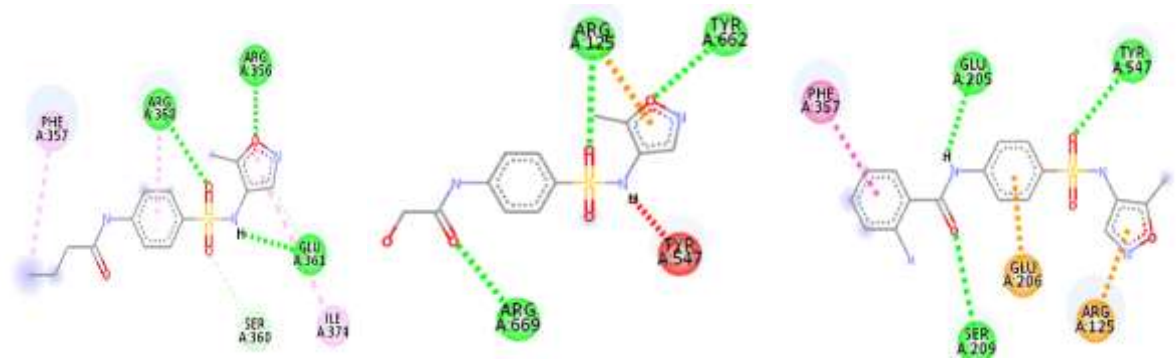

L_17 **L_18** **L_19**

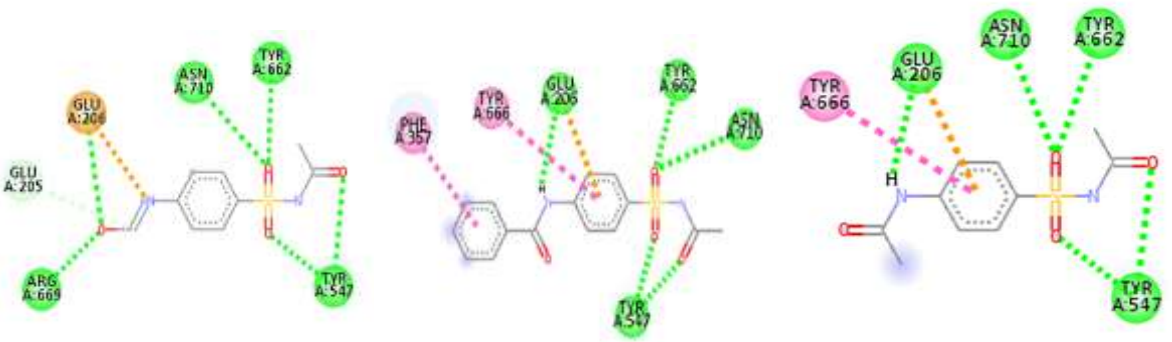

L_21 **L_22** **L_23**

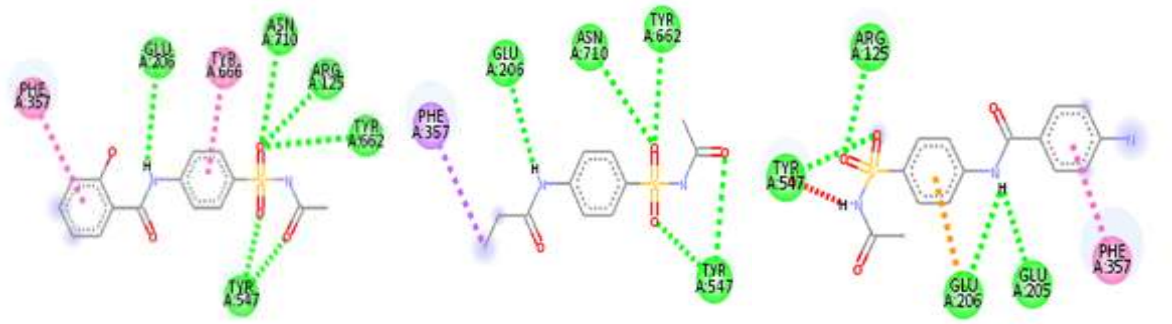

L_24 **L_25** **L_26**

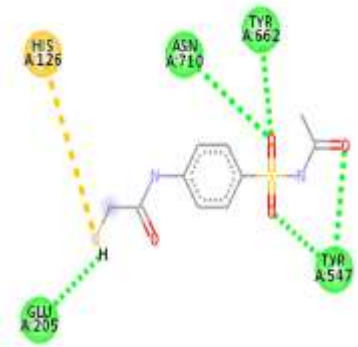

L_27

L_28

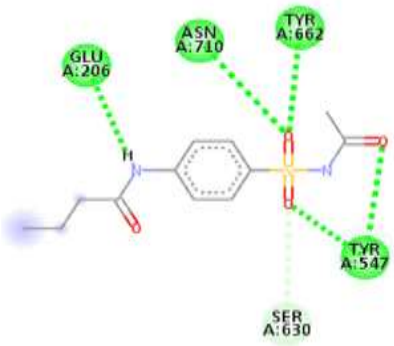

L_29

L_30

L_31

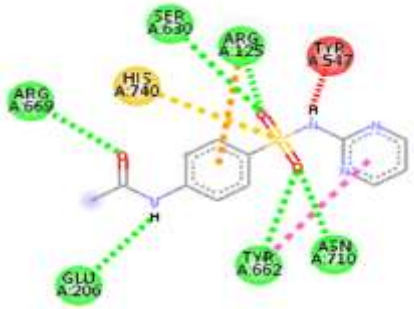

L_32

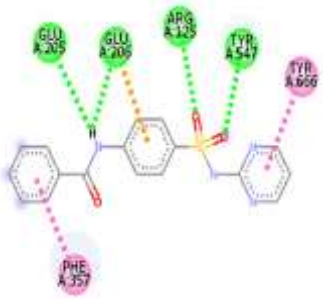

L_33

L_34

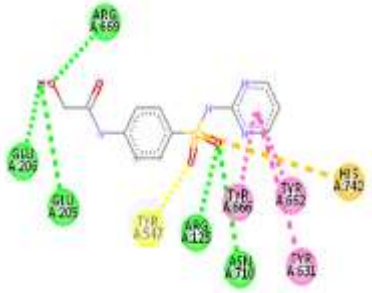

L_35

L_36

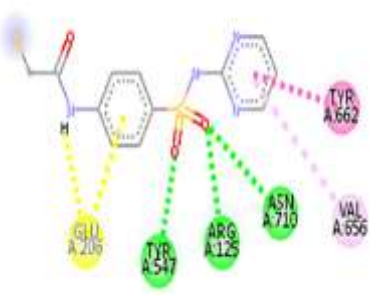

L_37

L_38

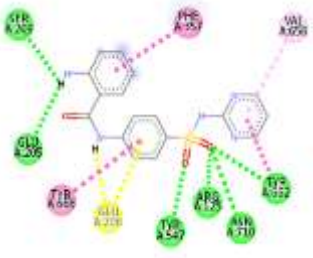

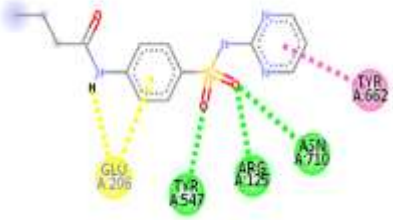

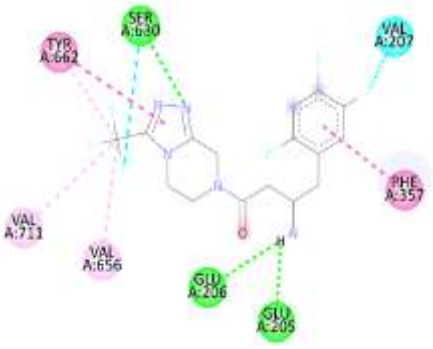

L_39 **L_40** **Sitagliptin**

Figure 4. Two-dimensional protein–ligand interaction diagrams of selected sulfamoyl phenyl derivatives and Sitagliptin docked into the DPP-4 active site (PDB ID: 2OQV), generated using BIOVIA Discovery Studio Visualizer.

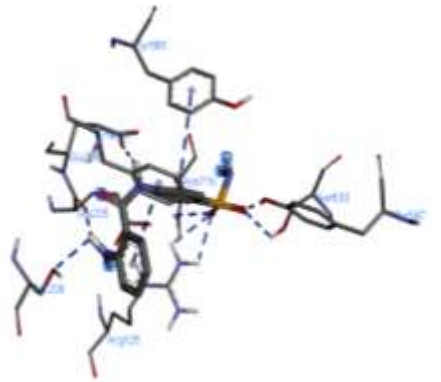

L_2

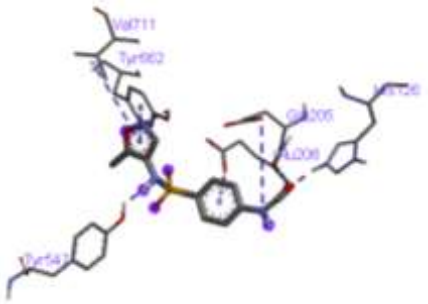

L_3

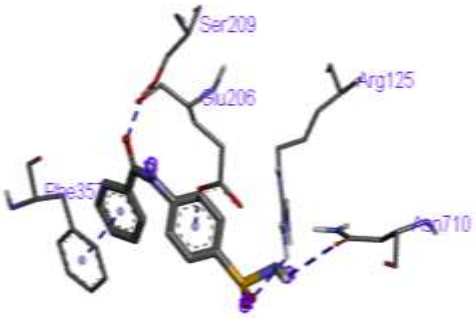

L_5

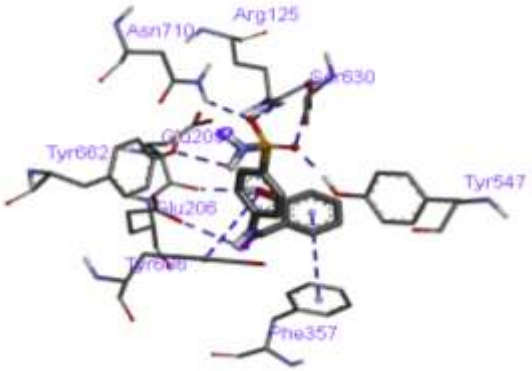

L_7

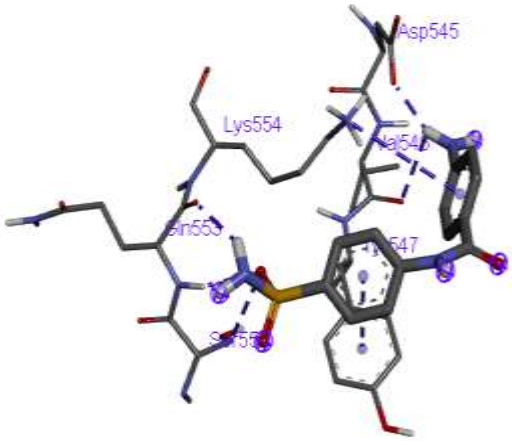

L_8

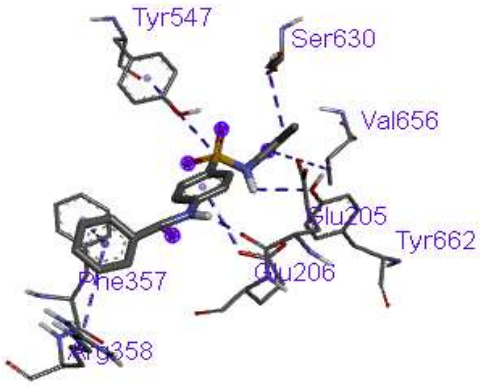

L_11

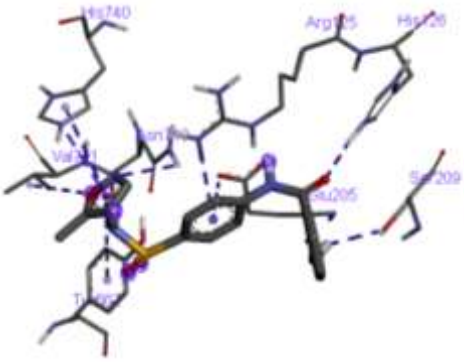

L_12

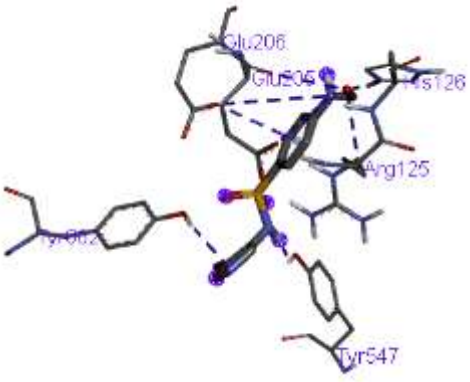

L_14

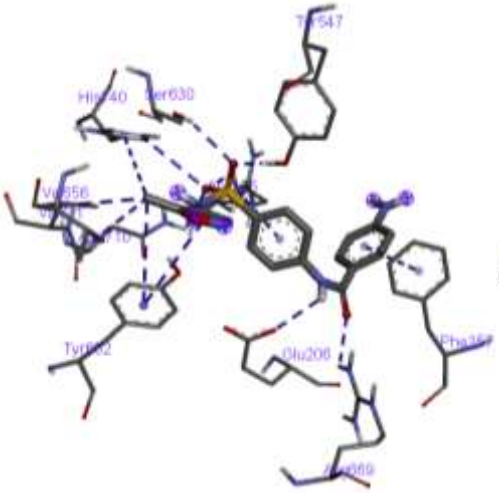

L_15

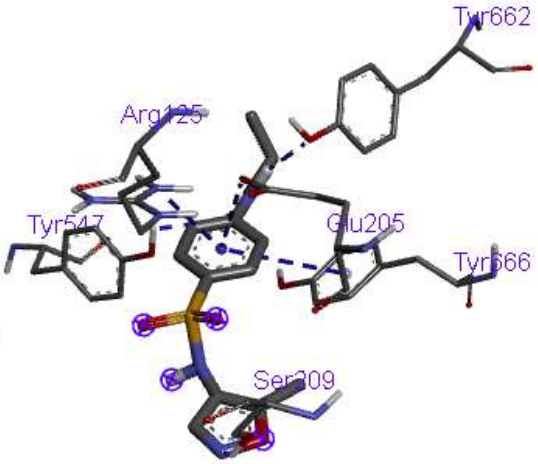

L_16

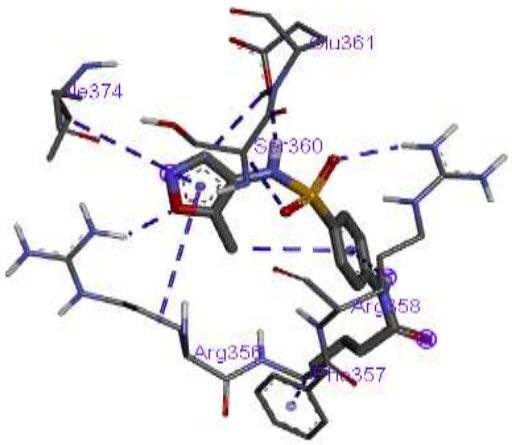

L_17

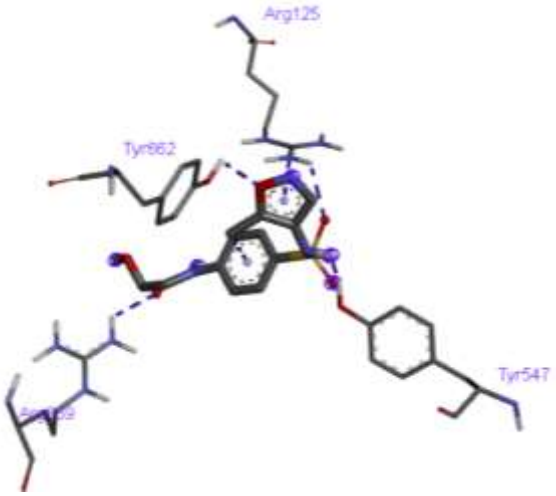

L_18

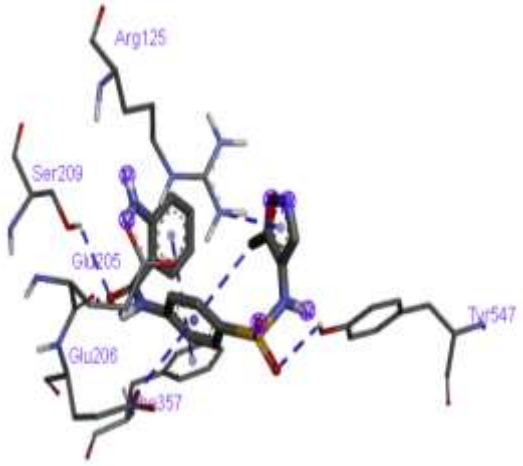

L_19

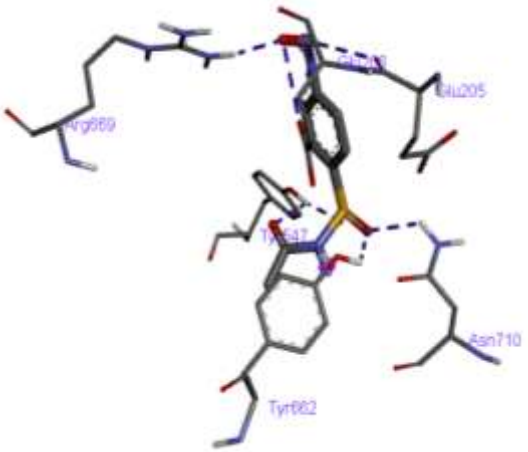

L_21

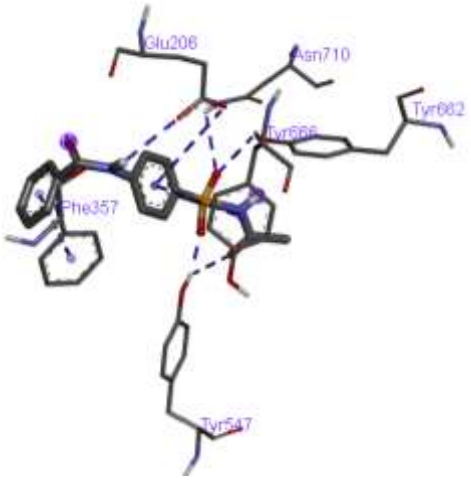

L_22

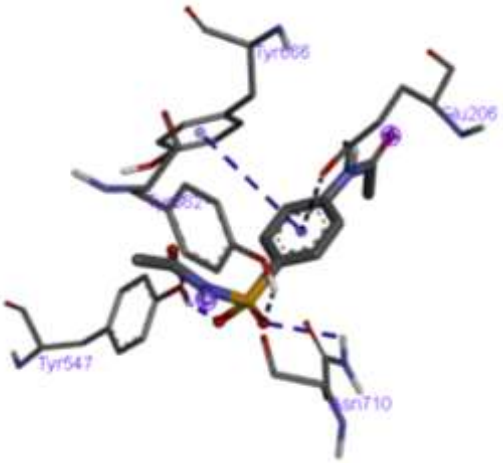

L_23

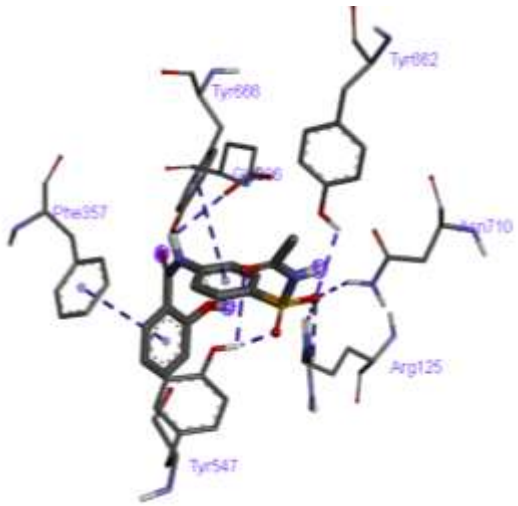

L_24

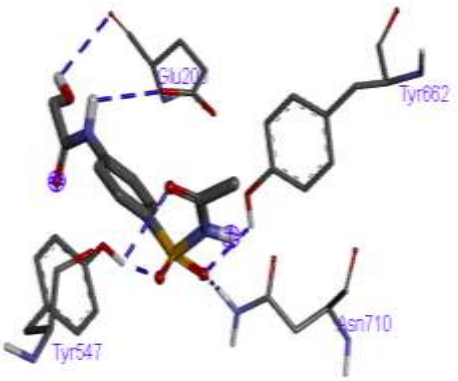

L_25

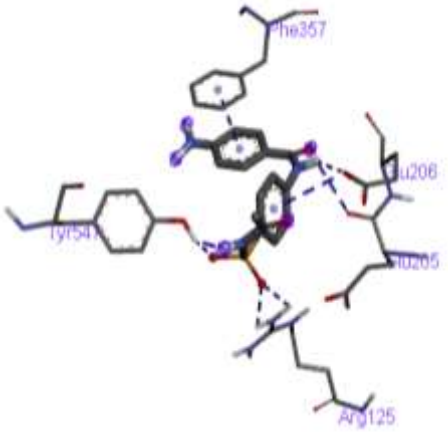

L_26

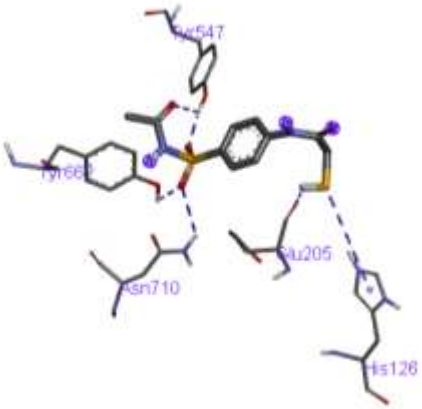

L_27

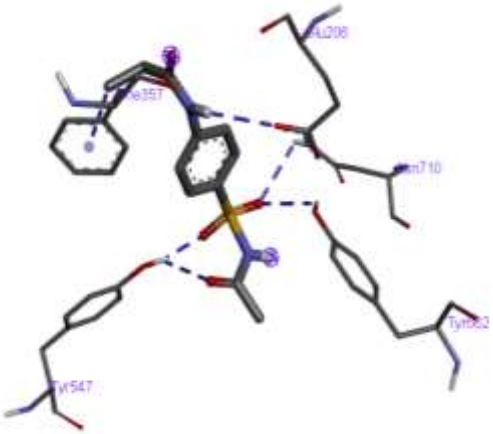

L_28

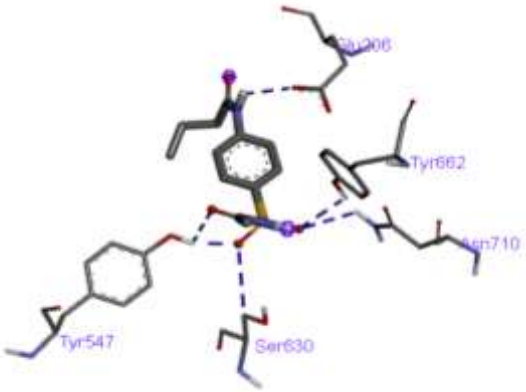

L_29

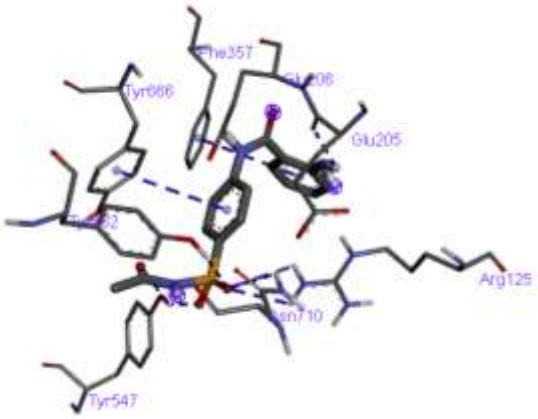

L_30

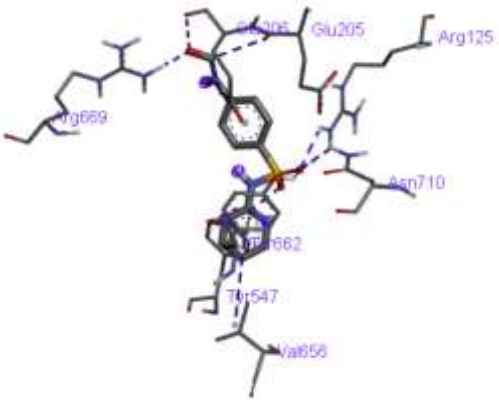

L_31

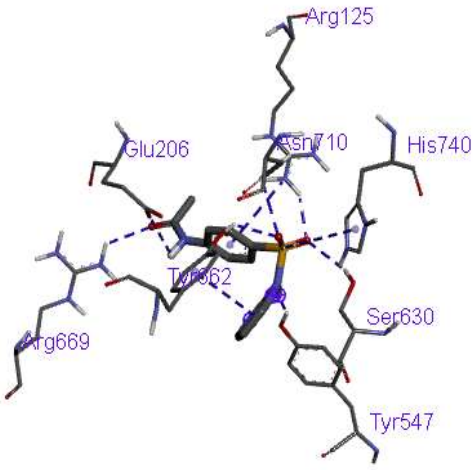

L_32

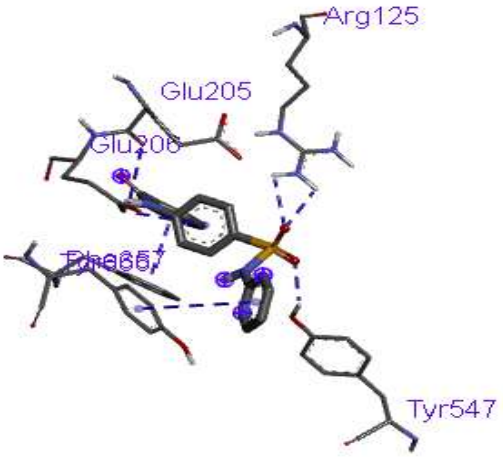

L_33

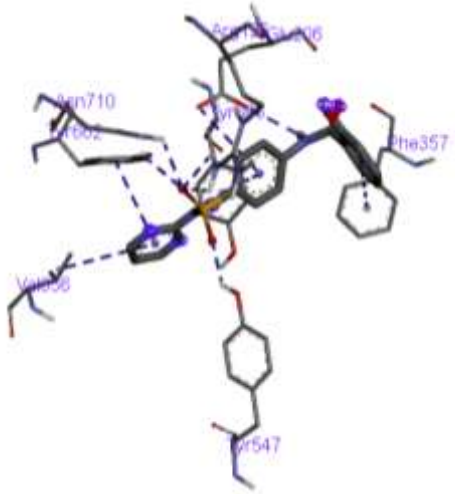

L_34

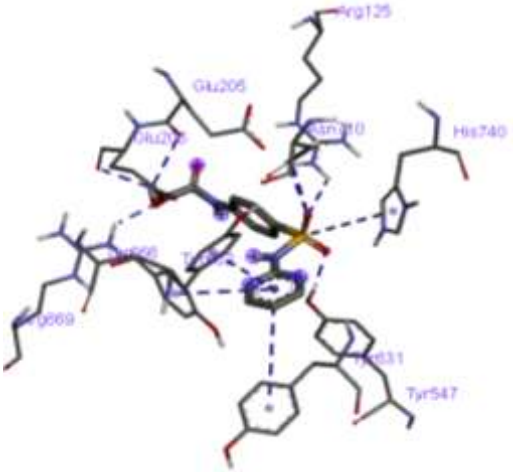

L_35

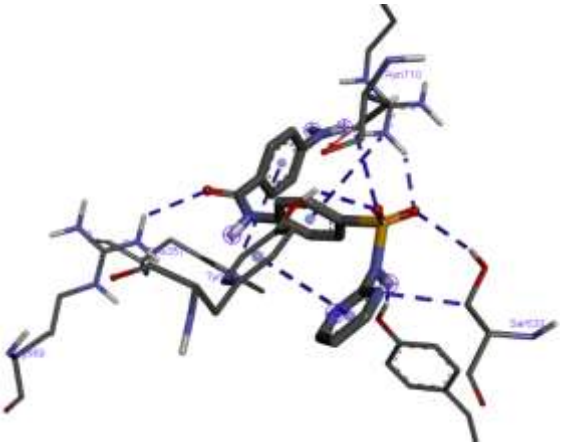

L_36

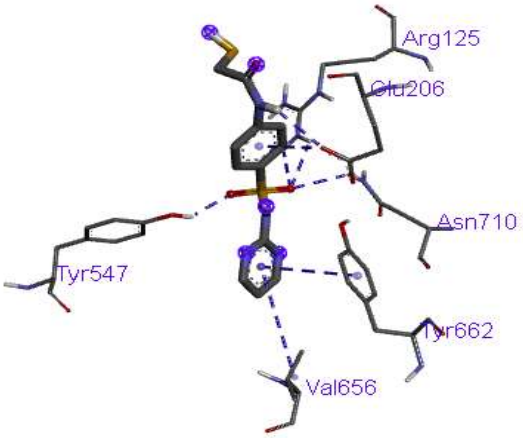

L_37

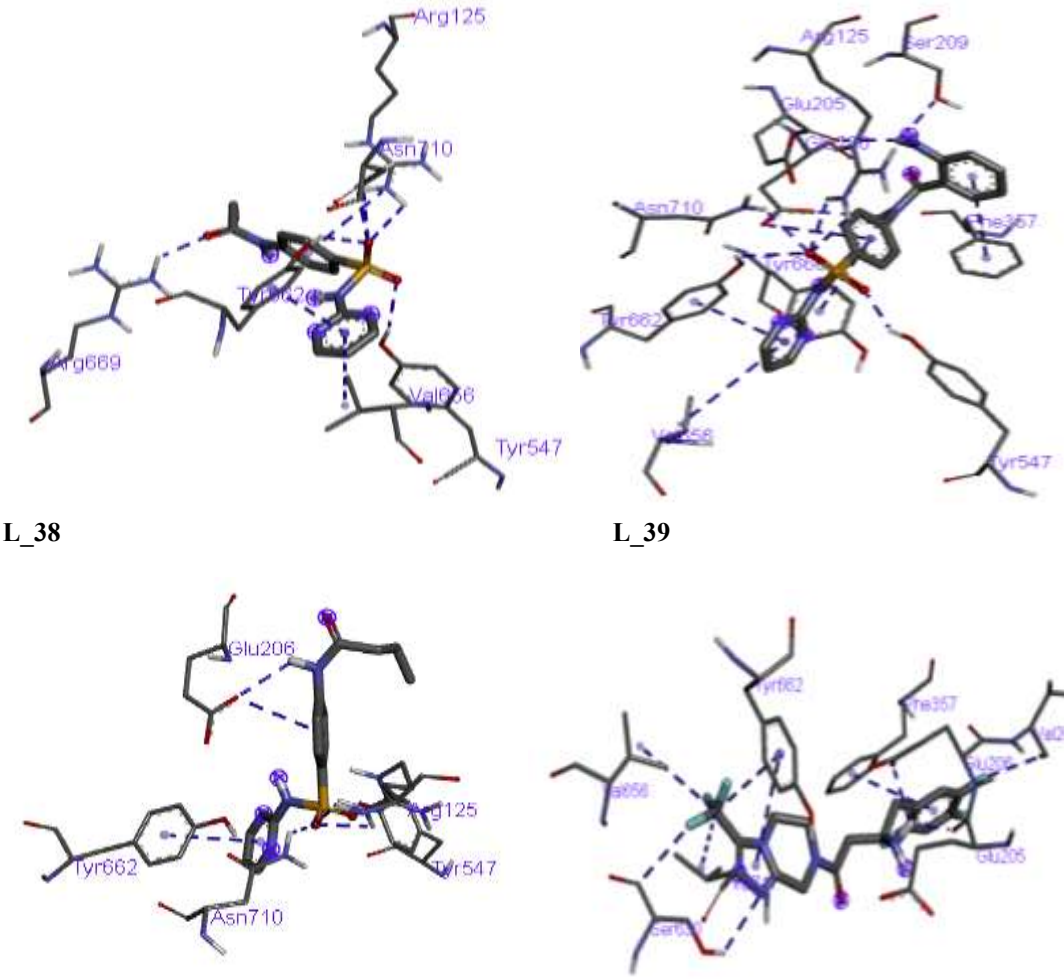

L_38 **L_39**

L_40 **Sitagliptin**

Figure 5: Three-dimensional protein–ligand interaction diagrams of selected sulfamoyl phenyl derivatives and Sitagliptin docked into the DPP-4 active site (PDB ID: 2OQV), generated using BIOVIA Discovery Studio Visualizer.

RADAR DATA

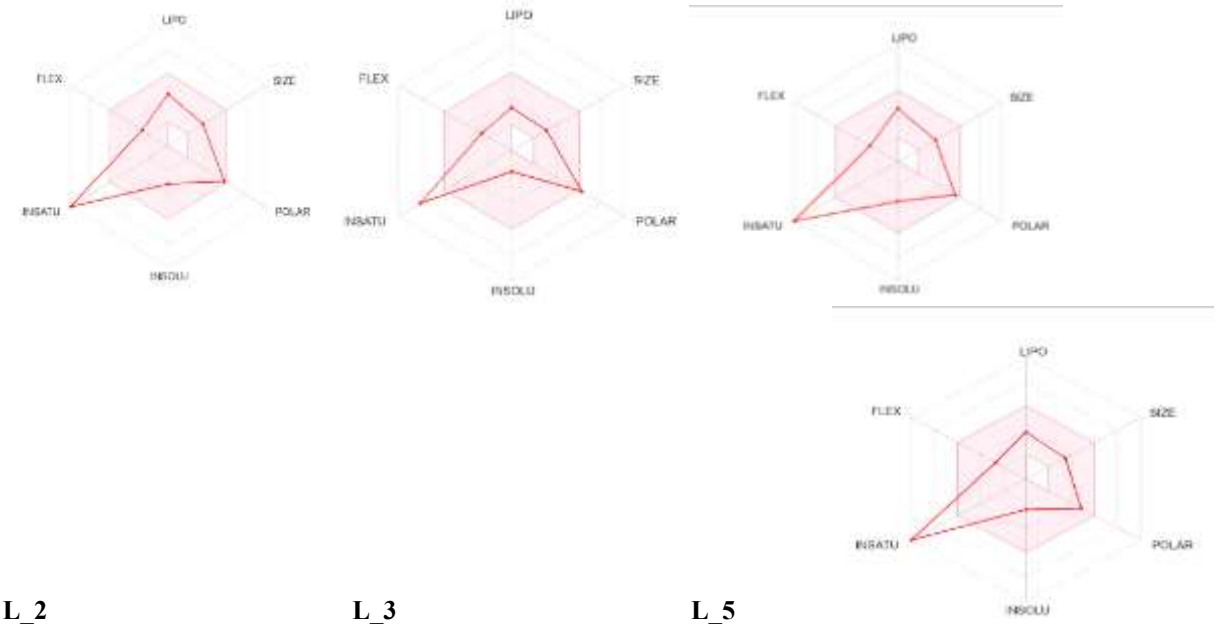

L_2 **L_3** **L_5**

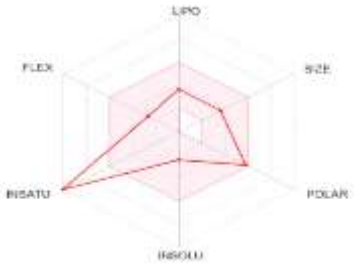

L_7

L_8

L_11

L_12

L_14

L_15

L_16

L_17

L_18

L_19

L_21

L_22

L_23

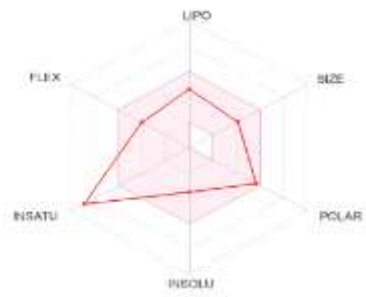

L_24

L_25

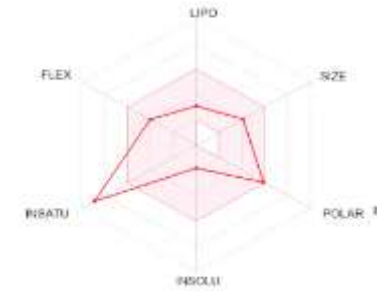

L_26

L_27

L_28

L_29

L_30

L_31

L_33

L_34

L_32

L_35

L_36

L_37

L_38

L_39

L_40

Sitagliptin

Figure 6: Comparative bioavailability radar plots of the designed sulfamoyl phenyl derivatives and standard DPP-4 inhibitor Sitagliptin generated using SwissADME

BOILED-Egg plot

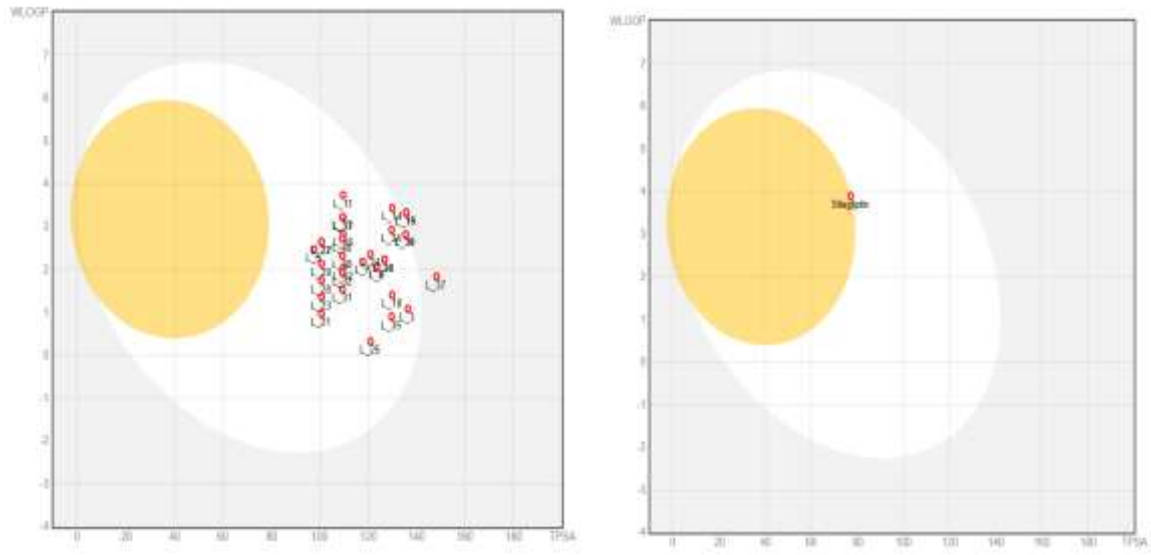

Figure 7: BOILED-Egg plot represented passive gastrointestinal absorption (HIA) in white region and brain penetration (BBB) in yellow region properties of designed sulfamoyl phenyl derivatives and Sitagliptin

4. CONCLUSION

This study presents a systematic in silico evaluation of 40 rationally designed sulfamoyl phenyl derivatives as potential DPP-4 inhibitors, integrating molecular docking, ADMET profiling, and multi-endpoint toxicity prediction within a single computational workflow. Molecular docking identified L_33 and L_11 as lead compounds achieving binding affinities of −9.7 and −9.3 kcal/mol — equalling or closely approaching the benchmark gliptin Sitagliptin — through coherent engagement of the DPP-4 catalytic and auxiliary binding residues, including GLU205, GLU206, SER630, PHE357, and TYR662. Pharmacokinetic evaluation confirmed that the majority of compounds comply with oral drug-likeness criteria, display high predicted GI absorption, and are unlikely to cause major CYP-mediated drug interactions. Toxicity assessment highlighted structurally distinct compounds (notably L_5 and L_8) with exceptionally clean predicted safety profiles, and furnished actionable structural guidance for addressing hepatotoxic and nephrotoxic liabilities observed in a subset of analogues.

Collectively, these computational findings position sulfamoyl phenyl derivatives as a chemically tractable and mechanistically well-grounded scaffold family for DPP-4 inhibitor discovery. The priority next steps are in vitro DPP-4 enzyme inhibition assays to validate predicted binding affinities, followed by cellular glucose-tolerance and insulin-secretion models to confirm target engagement and functional efficacy. Pharmacokinetic profiling in rodent models and comprehensive safety assessment — including Ames testing and hepatocyte cytotoxicity — will be essential before progression to pre-clinical in vivo studies. The computational blueprint established here provides a data-driven foundation for the iterative design and optimisation of this promising class of antidiabetic lead molecules.

5. ACKNOWLEDGMENTS

We are thankful to Dr. Ashish Srivastava PSIT, Kanpur and Mr. Shiwa Chaubey CSIR-National Botanical Research Institute, Lucknow, for providing the facility to learn and carry out the work.

6. FUNDING
No funding source applicable.

7. CONFLICTS OF INTERESTS
No declarations of interest were made.

8. AUTHORS' CONTRIBUTIONS
Dr. Kumud Madan conceived and supervised the study and served as the corresponding author. Shiwani Jaiswal carried out the molecular docking studies, ADMET and toxicity analyses, interpreted the data, and prepared the manuscript. Dr. Ashish Srivastava contributed to study design, data collection, and manuscript editing. Chandan Mondal helped in data interpretation and critical revision of the manuscript. Mrs.Shweta Yadav provided scientific guidance, reviewed the results, and critically revised the manuscript. All authors have read and agreed to the published version of the manuscript.

REFERENCES
1. Chaudhry CS. Emerging Diabetes Pandemic in India: A Case Study for an Integrative Approach [Internet]. Walden University ScholarWorks. Available from: https://scholarworks.waldenu.edu/dissertations.
2. Pradhan R. Incretin-based drugs and the incidence of skin cancer among patients with type 2 diabetes. 2022.
3. Havale SH, Pal M. Medicinal chemistry approaches to the inhibition of dipeptidyl peptidase-4 for the treatment of type 2 diabetes. Bioorg Med Chem. 2009;17(5):1783–802. doi:10.1016/j.bmc.2009.01.061.
4. Tomkin GH. Treatment of type 2 diabetes, lifestyle, GLP-1 agonists and DPP-4 inhibitors. World J Diabetes. 2014;5(5):636–642. doi:10.4239/wjd.v5.i5.636.
5. Cho YM, Merchant CE, Kieffer TJ. Targeting the glucagon receptor family for diabetes and obesity therapy. Pharmacol Ther. 2012;135(2):247–78. doi:10.1016/j.pharmthera.2012.05.009.
6. Saini K, Sharma S, Khan Y. DPP-4 inhibitors for treating T2DM — hype or hope? An analysis based on the current literature. Front Mol Biosci. 2023. doi:10.3389/fmolb.2023.1130625.
7. Aroor AR, Sowers JR, Jia G, DeMarco VG. Pleiotropic effects of the dipeptidyl peptidase-4 inhibitors on the cardiovascular system. Am J Physiol Heart Circ Physiol. 2014;307(4):H477–92. doi:10.1152/ajpheart.00209.2014
8. Drucker DJ. Dipeptidyl peptidase-4 inhibition and the treatment of type 2 diabetes: preclinical biology and mechanisms of action. Diabetes Care. 2007;30(6):1335–43. doi:10.2337/dc07-0228
9. Lambeir AM, Durinx C, Scharpé S, De Meester I. Dipeptidyl-peptidase IV from bench to bedside: an update on structural properties, functions, and clinical aspects of the enzyme DPP IV. Crit Rev Clin Lab Sci. 2003;40(3):209–94.
10. Pei Z, Li X, Von Geldern TW, et al. Discovery and structure–activity relationships of piperidinone- and piperidine-constrained phenethylamines as novel, potent, and selective dipeptidyl peptidase IV inhibitors. J Med Chem. 2007;50(8):1983–7. doi:10.1021/jm061436d
11. El-Saghier AM, Hashem H, Maher SA, et al. Design, synthesis, anticancer screening, and mechanistic study of spiro-N-(4-sulfamoyl-phenyl)-1,3,4-thiadiazole-2-carboxamide derivatives. Int J Mol Sci. 2025;26(2):863. doi:10.3390/ijms26020863
12. Durgun M, Turkmen H, Ceruso M, Supuran CT. Synthesis of 4-sulfamoylphenyl-benzylamine derivatives with inhibitory activity against human carbonic anhydrase isoforms I, II, IX and XII. Bioorg Med Chem. 2016;24(5):982–8. doi:10.1016/j.bmc.2016.01.020
13. Tuğrak M, Gül HI, Anil B, Gülçin İ. Synthesis and pharmacological effects of novel benzenesulfonamides carrying benzamide moiety as carbonic anhydrase and acetylcholinesterase inhibitors. Turk J Chem. 2020;44(6):1601–9. doi:10.3906/kim-2007-37
14. Singh P, Srivastava N, Ved A. Exploring the binding affinities of 2-methyl-N-(1,3-dioxoisoindolin-2-yl) benzamide derivatives as potent DPP-4 inhibitors. Res J Pharm Technol. 2025;18(9):4389–95. doi:10.52711/0974-360X.2025.00629
15. Singh SK. Innovations and Implementations of Computer Aided Drug Discovery Strategies in Rational Drug Design. Singapore: Springer; 2021. doi:10.1007/978-981-15-8936-2
16. Sukhachev VS, Dmitriev A V., Ivanov SM, Savosina PI, Druzhilovskiy DS, Filimonov DA, et al. Assessment of the Efficiency of Selecting Promising Compounds During Virtual Screening Based on Various Estimations of Drug-Likeness. Pharm Chem J. 2024 Dec 21;58(9):1388–96.
17. Kowalska M, Fijałkowski Ł, Nowaczyk A. eISNN 2391-8306 The journal has had 7 points in Ministry of Science and Higher Education parametric evaluation. Journal of Education [Internet]. 2018;8(12):2391–8306. Available from: http://dx.doi.org/10.5281/zenodo.2066519.

ABBREVIATIONS

ADA	Adenosine Deaminase
ADMET	Absorption, Distribution, Metabolism, Excretion and Toxicity
BBB	Blood–Brain Barrier
CYP	Cytochrome P450
DPP-4	Dipeptidyl Peptidase-4
GI	Gastrointestinal
GLP-1	Glucagon-Like Peptide-1
GIP	Glucose-Dependent Insulinotropic Polypeptide
LD	Lethal Dose
PDB	Protein Data Bank
PDBQT	Protein Data Bank, Partial Charge (Q) and Atom Type (T)
T2DM	Type 2 Diabetes Mellitus
TPSA	Topological Polar Surface Area
UFF	Universal Force Field
L_2	2-amino-N-(4-sulfamoylphenyl) benzamide
L_3	2-mercapto-N-(4-sulfamoylphenyl) acetamide
L_5	N-(4-(N-acetylsulfamoyl) phenyl) benzamide
L_8	4-amino-N-(4-sulfamoyl phenyl) benzamide
L_11	N-(4-(N-(5-methylisoxazol-4-yl) sulfamoyl) phenyl) benzamide
L_12	N-(4-(N-(5-methylisoxazol-4-yl) sulfamoyl) phenyl) formamide
L_14	2-hydroxy-N-(4-(N-(5-methylisoxazol-4-yl) sulfamoyl) phenyl) benzamide
L_15	4-amino-N-(4-(N-(5-methylisoxazol-4-yl) sulfamoyl) phenyl) benzamide
L_16	N-(4-(N-(5-methylisoxazol-4-yl) sulfamoyl) phenyl) propionamide
L_17	N-(4-(N-(5-methylisoxazol-4-yl) sulfamoyl) phenyl) butyramide
L_18	2-hydroxy-N-(4-(N-(5-methylisoxazol-4-yl) sulfamoyl) phenyl) acetamide
L_19	2-amino-N-(4-(N-(5-methylisoxazol-4-yl) sulfamoyl) phenyl) benzamide
L_21	N-((4-formamidophenyl) sulfonyl) acetamide
L_22	N-(4-(N-acetylsulfamoyl) phenyl) benzamide
L_23	N-((4-acetamidophenyl) sulfonyl) acetamide
L_24	N-(4-(N-acetylsulfamoyl) phenyl)-2-hydroxybenzamide
L_25	N-(4-(N-acetylsulfamoyl) phenyl)-2-hydroxyacetamide
L_26	N-(4-(N-acetylsulfamoyl) phenyl)-4-aminobenzamide
L_27	N-(4-(N-acetylsulfamoyl) phenyl)-2-mercaptoacetamide
L_28	N-(4-(N-acetylsulfamoyl) phenyl) propionamide
L_29	N-(4-(N-acetylsulfamoyl) phenyl) butyramide
L_30	N-(4-(N-acetylsulfamoyl) phenyl)-2-aminobenzamide
L_31	N-(4-(N-(pyrimidin-2-yl) sulfamoyl) phenyl) formamide
L_32	N-(4-(N-(pyrimidin-2-yl) sulfamoyl) phenyl) acetamide
L_33	N-(4-(N-(pyrimidin-2-yl) sulfamoyl) phenyl) benzamide
L_34	2-hydroxy-N-(4-(N-(pyrimidin-2-yl) sulfamoyl) phenyl) benzamide
L_35	2-hydroxy-N-(4-(N-(pyrimidin-2-yl) sulfamoyl) phenyl) acetamide
L_36	4-amino-N-(4-(N-(pyrimidin-2-yl) sulfamoyl) phenyl) benzamide
L_37	2-mercapto-N-(4-(N-(pyrimidin-2-yl) sulfamoyl) phenyl) acetamide
L_38.	N-(4-(N-(pyrimidin-2-yl) sulfamoyl) phenyl) propionamide
L_39.	2-amino-N-(4-(N-(pyrimidin-2-yl) sulfamoyl) phenyl) benzamide
L_40	N-(4-(N-(pyrimidin-2-yl) sulfamoyl) phenyl) butyramide